



Treball Final de Grau

**Kinetic study on the air oxidation of Fe(II) bis-thiosemicarbazones.
Estudi cinètic de l'oxidació de compostos bis-tiosemicarbazona
de Fe(II) per l'aire.**

Miguel Agustín González Noguera

January 2017



UNIVERSITAT DE
BARCELONA

B:KC Barcelona
Knowledge
Campus
Campus d'Excel·lència Internacional

Aquesta obra esta subjecta a la llicència de:
Reconeixement–NoComercial–SenseObraDerivada



<http://creativecommons.org/licenses/by-nc-nd/3.0/es/>

You don't get what you want in life. You get who you are!

Les Brown

En primer lugar, me gustaría agradecer a Manel y Marta por su ayuda y paciencia a lo largo de todo este trabajo, así como a Montse por su ayuda en la síntesis de los complejos.

Seguidamente, a Jordi y Heribert por estos años de amistad, a la gente con la que he compartido clases y laboratorios a lo largo de la carrera y en especial, a Victor, Edu y Diego por todos esos momentos juntos. Sé que a donde vayáis dejaréis vuestra huella.

Finalmente, a la gente que ha sido más importante en este trabajo: mi abuela, mi tío Francisco, mi hermana y mis padres, por haber hecho de mi un adulto orgulloso de sus valores.

REPORT

CONTENTS

1. SUMMARY	3
2. RESUM	5
3. INTRODUCTION	7
3.1. Electronic structure	9
3.2. Electronic spectra of complexes	10
3.3. Electronic transfer processes	11
3.3.1. Inner-sphere electron transfer	11
3.3.2. Outer-sphere electron transfer	12
3.4. Marcus theory for outer-sphere reactions	12
4. OBJECTIVES	15
5. EXPERIMENTAL SECTION	16
5.1. Chemicals and reagents	16
5.1.1. Preparation of stock solutions	16
5.1.2. Thiosemicarbazone ligands: General procedure	16
5.1.3. Fe ^{II} and Fe ^{III} thiosemicarbazone complexes: General procedure	17
5.2. Physical methods	18
5.3. Kinetic studies	20
5.3.1. Variable-temperature kinetic studies	20
5.3.2. Variable-pressure kinetics studies	20
5.3.3. Software used for data analysis	21
6. RESULTS	22
6.1. Modelling the time-resolved spectral changes: reaction rates	22
6.2. Study of the effect of temperature	24
6.3. Study of the effect of pressure	25
6.4. Study of the effect of pH on the rate constant in aqueous solutions	28

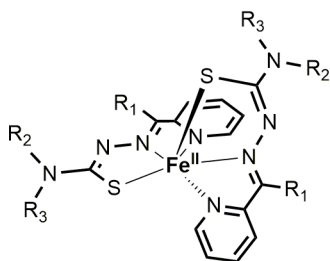
7. DISCUSSION	30
7.1. Observed spectral changes in methanol solution	30
7.2. Mechanistic classification	31
7.3. Relation of the kinetic and activation parameters with the standard reduction potential in methanol solution	32
7.4. Interpretation of the effect of pH on the rate constant in aqueous solution	35
8. CONCLUSIONS	37
9. REFERENCES AND NOTES	38
10. ACRONYMS	41
APPENDICES	42
Appendix 1: Data used for kinetic studies on the temperature dependence in MeOH solutions	43
Appendix 2: Data used for preliminary studies on the relationship between the rate constant and pH in aqueous solution	46

1. SUMMARY

Thiosemicarbazones have been considered as antiviral, antibacterial, and antineoplastic agents in multiple studies through the years. Furthermore, their ability as excellent chelators for iron in its ferrous and ferric forms, make them very promising drugs in anti-cancer therapy from a polypharmacological perspective, as they can fight multiple molecular targets via iron deprivation and cell cytotoxicity.

By changing the structure of these chelating compounds the chemical properties of their Fe complexes can be altered and in turn, their biological activity. Having this in mind, studying the effects of structural changes via kinetic experimentation is essential to help in the design of future generations of thiosemicarbazones with enhanced properties by their own or their complexes.

The work here presented studies the oxidation of Fe(II) bis-thiosemicarbazone complexes from the ApT and DpT series by oxygen in solution from a kinetic perspective. The dependence of the reaction rate constant on different temperature and pressure for MeOH solutions and the effect of pH in aqueous solutions will be discussed. A basic mechanistic approach will also be used to interpret the kinetic and activation parameters obtained.



· ApT series ($R_1 = \text{CH}_3$)

$[\text{Fe}^{\text{II}}(\text{ApT})_2]$: $R_2 = \text{H}$, $R_3 = \text{H}$

$[\text{Fe}^{\text{II}}(\text{Ap4mT})_2]$: $R_2 = \text{CH}_3$, $R_3 = \text{H}$

$[\text{Fe}^{\text{II}}(\text{Ap44mT})_2]$: $R_2 = \text{CH}_3$, $R_3 = \text{CH}_3$

· DpT series ($R_1 = \text{py}$)

$[\text{Fe}^{\text{II}}(\text{DpT})_2]$: $R_2 = \text{H}$, $R_3 = \text{H}$

$[\text{Fe}^{\text{II}}(\text{Dp4mT})_2]$: $R_2 = \text{CH}_3$, $R_3 = \text{H}$

$[\text{Fe}^{\text{II}}(\text{Dp44mT})_2]$: $R_2 = \text{CH}_3$, $R_3 = \text{CH}_3$

Fe(II) bis-thiosemicarbazone complexes used in this study

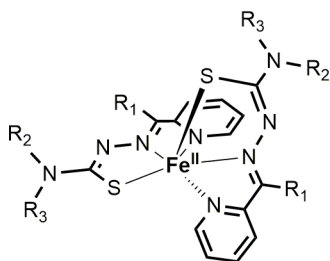
Keywords: Fe(II) bis-thiosemicarbazone complexes, kinetic study, oxidation, thiosemicarbazone chelators, iron, mechanism.

2. RESUM

Les tiosemicarbazones han estat considerades com a agents antivirals, antibacterials i antineoplàstics en múltiples estudis al llarg dels anys. A més, la seva habilitat com a excel·lents quelants del ferro en les seves formes ferrosa i fèrrica, fan que siguin medicaments molt prometedors quant a la teràpia anti-càncer des d'una perspectiva polifarmacològica, degut a que poden lluitar contra múltiples dianes moleculars via privació de ferro i citotoxicitat cel·lular.

Canviant l'estructura d'aquests compostos quelants es poden alterar les propietats químiques dels seus compostos de Fe i d'aquesta manera, la seva activitat biològica. Amb això en ment, estudiant els efectes dels canvis estructurals via experimentació cinètica és essencial per ajudar en el disseny de futures generacions de tiosemicarbazones amb millors propietats per si mateixes o pels seus complexos.

El treball aquí presentat estudia l'oxidació dels complexos bis-tiosemicarbazona de Fe(II) de les sèries ApT i BpT per oxigen en sol·lució des d'una perspectiva cinètica. La dependència de la constant de velocitat de la reacció amb la temperatura i la pressió per solucions amb MeOH, i l'efecte del pH en solucions aquoses serà tractat. Un plantejament mecanístic bàsic també serà utilitzat per interpretar els paràmetres cinètics i d'activació obtinguts.



· ApT series ($R_1 = \text{CH}_3$)

$[\text{Fe}^{\text{II}}(\text{ApT})_2]$: $R_2 = \text{H}$, $R_3 = \text{H}$

$[\text{Fe}^{\text{II}}(\text{Ap4mT})_2]$: $R_2 = \text{CH}_3$, $R_3 = \text{H}$

$[\text{Fe}^{\text{II}}(\text{Ap44mT})_2]$: $R_2 = \text{CH}_3$, $R_3 = \text{CH}_3$

· DpT series ($R_1 = \text{py}$)

$[\text{Fe}^{\text{II}}(\text{DpT})_2]$: $R_2 = \text{H}$, $R_3 = \text{H}$

$[\text{Fe}^{\text{II}}(\text{Dp4mT})_2]$: $R_2 = \text{CH}_3$, $R_3 = \text{H}$

$[\text{Fe}^{\text{II}}(\text{Dp44mT})_2]$: $R_2 = \text{CH}_3$, $R_3 = \text{CH}_3$

Complexos bis-tiosemicarbazona de Fe(II) utilitzats en aquest estudi

Paraules clau: Complexos bis-tiosemicarbazona de Fe(II), estudi cinètic, oxidació, quelants tiosemicarbazona, ferro, mecanisme.

3. INTRODUCTION

Thiosemicarbazones (TSCs) have been considered of particular interest in medicinal chemistry due to their anticancer, antibacterial and antiviral activity.¹ These compounds have a long history in medical studies, dating back to the 1950s, when they were discovered to be antileukemic agents, an effect attributed to their inhibition of the enzyme ribonucleotide reductase (RR^α). This enzyme is responsible for catalyzing the rate-limiting step of DNA synthesis of converting ribonucleotides to the corresponding 2'-deoxyribonucleotides.²

In recent years, studies have suggested that the inhibition of RR^α may be caused by Fe deprivation,³ which is responsible for electron transfer processes due to cycling between its ferrous and ferric states in the active site (R_2) of the enzyme.⁴ Precisely, this ability of gaining and losing electrons makes Fe an essential component in many biological processes, such as oxygen transport, energy metabolism and DNA synthesis. However, high concentrations of Fe may also lead to the undesired release of reactive oxygen species (ROS), namely superoxide and hydroxyl radicals, which are also highly cytotoxic.⁵

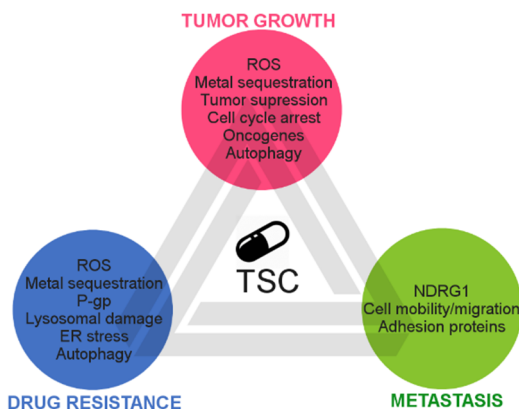


Figure 1. Polypharmacological effects of thiosemicarbazones for tumor growth, drug resistance and metastasis by different molecular targets. ER Stress: Endoplasmic reticulum stress. P-gp: P-glicoprotein 1 NDRG: N-myc downstream regulated gene (protein) ROS: Reactive oxygen species. (Image adapted from Jansson *et al.*, ref. 6)

The iron depletion properties of TSCs are directly related to their ability as excellent chelators for both Fe(II) and Fe(III), forming neutral or monopositive complexes at physiological pH that are also redox-active.⁷ This versatility gives thiosemicarbazones a “double punch” effect: the first punch would be their ability to bind iron, which is crucial for neoplastic cell growth/proliferation, and the second would be their redox active capability to reduce oxygen to form ROS leading to cellular death. Moreover, they are very promising drugs from a polypharmacological perspective as they can fight against tumor growth, metastasis, and drug resistance through multiple molecular targets (Fig.1).⁶

By changing the structure of thiosemicarbazones and their iron complexes it is possible to tune some of their chemical properties and in turn, their biological activity.⁸ In this study, the relationship between the structure and chemical properties of Fe(II) bis-thiosemicarbazone complexes from the ApT and DpT series (Fig. 2) will be examined from a kinetic perspective. Particularly, the kinetic study of the oxidation of the $[\text{Fe}^{\text{II}}(\text{TSC})_2]$ complexes by oxygen in solution will be conducted. The information of this type of studies is of important relevance for the design of future generations of thiosemicarbazone ligands with enhanced properties by its own or as ligands for iron complexes.

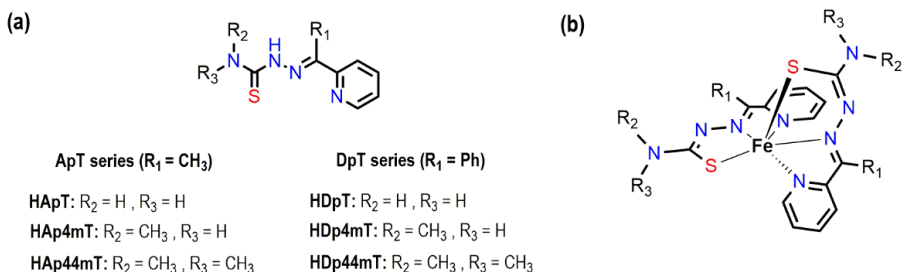


Figure 2. (a) Structural formulae of the thiosemicarbazone chelators used in this study: 2-acetylpyridine thiosemicarbazone (HApT), 2-acetylpyridine 4-methylthiosemicarbazone (HAp4mT), 2-acetylpyridine 4,4-dimethylthiosemicarbazone (HAp44mT), di-2-pyridyl thiosemicarbazone (HDpT), di-2-pyridyl 4-methylthiosemicarbazone (HDp4mT) and di-2-pyridyl 4,4-dimethylthiosemicarbazone. (HDp44mT)

(b) Stable Fe(II) complexes of the studied ligands.

In the following subsections, a brief overview on some important concepts in the field of coordination chemistry, kinetics and mechanisms relevant to the study carried out is presented.

3.1. ELECTRONIC STRUCTURE

The classical and simplified models used in coordination chemistry to explain the electronic structure of transition metal complexes are crystal field theory and ligand field theory. For qualitative purposes, the crystal field theory will be used throughout the report to give a basic overview on electronic structure. Nevertheless, it should not be taken as a complete and comprehensive interpretation; it simply collects the essential concepts that explain the structure and properties of d-metal complexes.

Crystal field theory (CFT) is a model that describes the loss of degeneracy of the d orbitals in transition metal complexes, thus explaining some of their inherent properties such as reactivity, stability, magnetism, and color.

CFT considers the ligands as negative point charges (uniformly charged spheres) that interact with a central metal cation. This electrostatic approach uses Coulomb's law to consider repulsive and attractive interactions. Taking into account that d-orbitals do not have spherical symmetry, their geometries and orientations in the planes must be considered for the breaking of their energy degeneration.

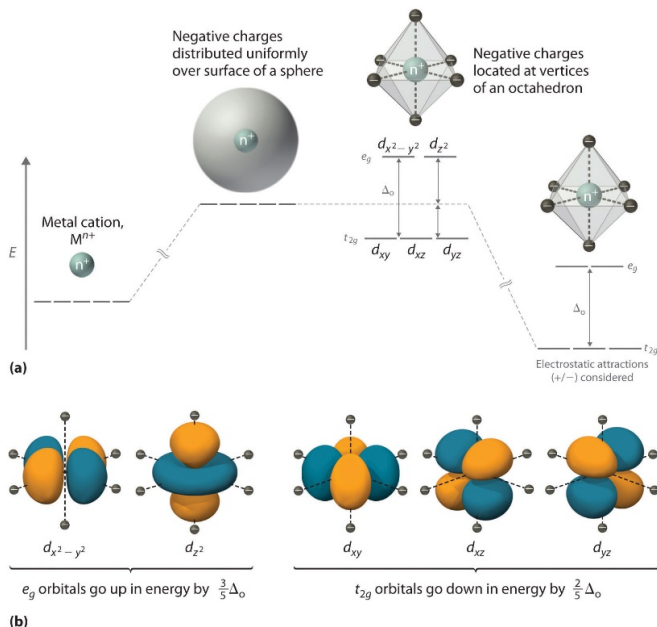


Figure 3. (a) Diagram of orbital energy for an octahedral environment, according to CFT (b) Spatial arrangement of the base d orbitals. (Image extracted from Lancashire et al., ref 9)

As a result of the splitting of the degenerate d-orbitals, complexes of transition metals with more than three d-electrons can display two electronic arrangements; pairing with an electron in the lowest energy orbitals (t_{2g}), low spin/strong field; or filling one of the higher energy orbitals (e_g), high spin/weak field. Both situations are illustrated in Figure 4:

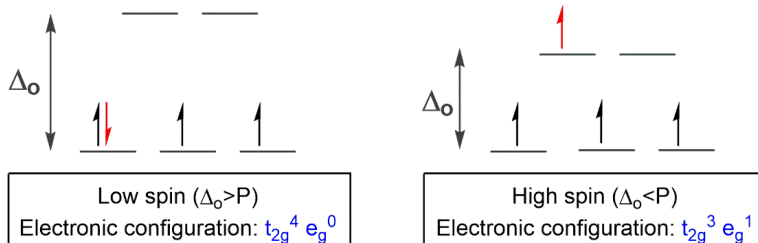


Figure 4. Possible electronic configurations for an Oh transition metal complex with four d-electrons.

The value of Δ_o (Oh geometry) depends on the nature of the metal center. Higher oxidation states of the metal increase the crystal field splitting. Conversely, the metals from the second and third transition series increase Δ_o because of the higher interactions caused by the larger metal ions.⁹ In both cases, a decrease in bond length between the metal and the ligand is a consequence of higher interaction energies.

The effect of ligands on the crystal field strength is also rather important in the value of the energy splitting of the d orbital degeneracy: its quantification on Δ_o is collected in the spectrochemical series ordered from lower to higher transition energies, as illustrated in Fig. 5.

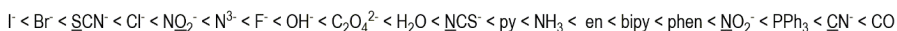


Figure 5. Spectrochemical series. Underlined ligands denote the donor atom.

3.2. ELECTRONIC SPECTRA OF COMPLEXES

Transition metal complexes present a wide array of colors based on changes in the oxidation states of the metal, the acceptor/donor character of the sigma and pi orbitals of the ligand and the geometric arrangement of the molecule. Two types of transitions are identified as being responsible of color: d-d transitions and charge-transfer.

When the energy of a transition in the absorption spectra of a transition metal complex is associated with its corresponding value of Δ_o , the transitions are said to be d-d. These bands are a result of vibronic-coupled electronic transitions caused by a disruption in the center of symmetry of the d-orbitals.¹⁰ Considerations on the electron-electron repulsions and the theory of orbitals have to be made in order to interpret these bands.

The other type of electronic transitions responsible for some of the bands in the visible or near UV region are those between orbitals with different character (metal or ligand origin), known as charge-transfer (CT) bands. This is the reason why some complexes present intense coloration despite only having the above mentioned forbidden transitions between the d-orbitals. Two types of CT can be identified: metal-to-ligand charge transfer (MLCT), for cases with metals in low oxidation states and ligands with acceptor orbitals at low energies; and ligand-to-metal charge transfer (LMCT) for metals with high oxidation states and ligands with electrons in non-bonding orbitals at relatively high energies.

3.3. ELECTRON TRANSFER PROCESSES

Electron transfer reactions for inorganic complex systems involve the transfer of one electron from a reducing to an oxidizing agent without the participation of an intermediate solvated electron. The reactions have been described (including two Nobel prizes) as occurring via two types of mechanisms that have been labeled as inner- and outer- sphere, depending on the type of activation needed for the process to take place.

3.3.1. Inner-sphere electron transfer

Inner sphere mechanisms have been traditionally described as those where a bridging ligand is formed between two metal centers before going to the transition state of the proper electron transfer. In recent years, this definition has been expanded to any situation where the interactions between the donor and acceptor centers in the transition state are significant.¹¹

The first step of this mechanism involves a substitution of/by a ligand (L), followed by the formation of a precursor complex where the two metal centers are joined through the formation of a bridge by the mentioned ligand. Then, the electron transfer may happen easily through the bridging group to form a successor complex (Fig. 6).¹² From this point, three possible products are possible to appear depending on the lability of the species formed.

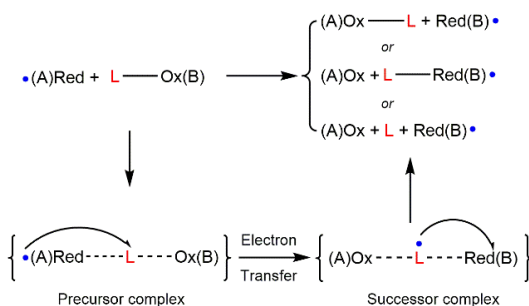


Figure 6. Simplified inner-sphere mechanism and possible products that can be obtained. The rate of the process relies heavily on the labile/inert nature of the reactants as well as on the reactivity of the bridging ligand.

3.3.2. Outer-sphere electron transfer

For outer sphere mechanisms, the coordination sphere of both oxidant and reductant remain unchanged during the full electron transfer process (Figure 7). An electrostatic or solvent cage approach has to be considered to explain the initial behavior of these systems, where the acceptor and donor are considered to behave as hard charged spheres.¹³ Nevertheless, due to the lack of sphericity in the charge distribution of both reactants a productive orientation is expected to be crucial once inside the solvent cage formed.

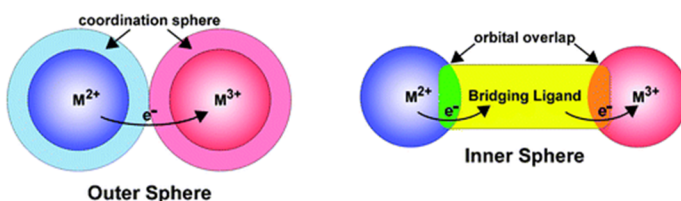
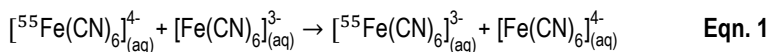


Figure 7. Simplified diagram showing the differences between outer-sphere (left) and inner-sphere (right) mechanisms. (Image extracted from Holliday *et al.*, ref. 13)

3.4. MARCUS THEORY FOR OUTER-SPHERE REACTIONS

Due to the fact that the electronic configuration of the coordination complexes of the studied Fe (II) complexes are low spin t_{2g}^6 (thus kinetically inert) and do not have any vacant coordination sites, the initial approximation for the reactions studied corresponds to an outer-sphere mechanism. For this reason, an overview on the theoretical development of the Marcus theory of electron transfer for the studied systems will be considered.

Early experimentation in electron transfer reactions on outer-sphere redox mechanisms involved the use of isotopic labeling exchange reactions in aqueous solution. These reactions are very simple, with the reactants and products being the same and no bonds being broken or formed. Consequently, the reactions have to occur simply due to the rearrangement of the full system involved in the process. An example is the self-exchange reaction of ferrocyanide and ferricyanide ions in aqueous solution:



Marcus described these systems as having a free energy that was a function of the many coordinates of position and orientation for the molecules of the solvent, and the vibrational coordinates of the reactants, among others. The Franck-Condon principle, fundamental to both inner- and outer-sphere approaches, states that electrons move much faster than the nuclei, thus internuclear distances are to remain the same during the proper electron transfer. For electron transfer following this principle and considering the laws of conservation of energy, changes in the orientation of the solvent molecules and in bond lengths of the coordination sphere had to be made before and after the instant of the electron being transferred from reductant to oxidant.

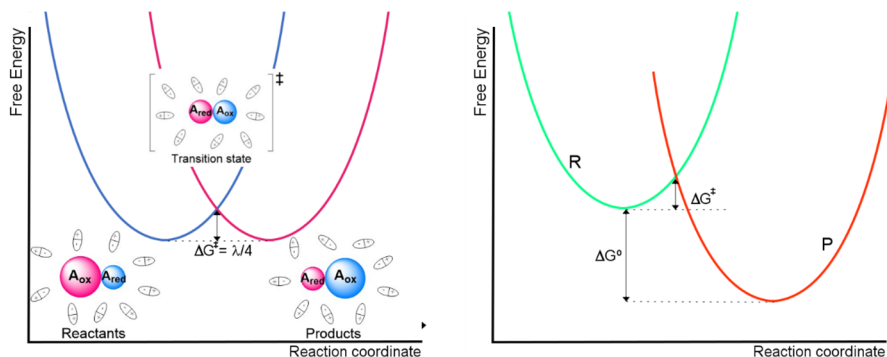
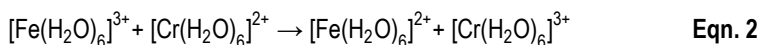


Figure 8. Simplified free energy curves for a self-exchange reaction (left) and a cross-reaction (right) under adiabatic conditions. P: Products + solvent, R: Reactants + solvent.

The free energy plot for the above-mentioned reaction was thus expected to have the form of Fig. 8. The illustration corresponds to the case where electronic coupling is not to be neglected (adiabatic conditions): the solvent molecules reorganize and the reactants reorient upon electron transfer, which occurs in the intersection of the potential wells with no structural

changes in the system, and they finally experience a relaxation to reach the products. Non-adiabatic conditions (weak coupling) would not present the intersection and the probabilities of the electron being transferred would have to be obtained using quantum mechanical calculations.¹⁵

Redox reactions between two different redox systems are known as cross-reactions. The free energy plot for these reactions is illustrated in Fig. 8. For these reactions, the net free energy change (ΔG^0) is an additional factor that affects the rate of the electron transfer.¹⁶ An example of cross-exchange reactions is the following:



Marcus' hypotheses for the above-mentioned reactions far from the diffusion limit introduce an activation barrier (ΔG^\ddagger) that includes the reorganization of bonds and angles of the reactants, and the rearrangement of the solvent on going to the transition state.¹⁷ The term that includes these factors is the reorganizational term (λ): for self-exchange reactions ΔG^\ddagger is equal to $\lambda/4$. For cross-reactions it includes ΔG^0 , and is expressed as:

$$\Delta G^\ddagger = \frac{\lambda}{4} \left(1 + \frac{\Delta G^0}{\lambda} \right)^2 \quad \text{Eqn. 3}$$

Moreover, the adiabatic nature of the electron transfer allows the use of the Eyring equation and the transition state theory to make predictions of the reaction rate constant (k). The transmission coefficient (ρ) in this equation becomes unity and simplifies the expression to the form:

$$k = \frac{k_B T}{h} \exp\left(\frac{-\Delta G^\ddagger}{RT}\right) \quad \text{Eqn. 4}$$

Where:

k_B : Boltzmann's constant

h : Planck's constant

R : Ideal gas constant

Other implications of the Marcus Theory is the Marcus cross-relationship that allow the reaction rate constant to be calculated from the relationship between the rate constants of the self-exchange reactions of the involved species and the corresponding equilibrium constants.¹³ For a reaction of the oxidant A[•] and a reductant B of the form A[•] + B → A + B[•]:

$$k_{AB} = (k_{AA} k_{BB} K_{AB} f)^{1/2} \quad \text{Eqn. 5}$$

Where:

k_{AA} and ***k_{BB}*** : the self-exchange reaction rate constants

K_{AB}: equilibrium constant (redox reaction).

f: term that involves the collision frequencies (simplified as unity for symmetrical charge equations).

4. OBJECTIVES

The aim of this work is to conduct a series of kinetic studies to give some insight on the characteristics of the chemical reaction, reaction mechanism and transition state for the oxidation of Fe(II) bis-thiosemicarbazone complexes by atmospheric oxygen. For this purpose, a set of specific objectives was defined, as follows:

- Determine the chemical behavior of the systems by means of UV-Vis spectroscopy.
- Analyze the dependence of the pseudo-first order reaction rate constants with the concentration of O₂ in MeOH in order to determine the rate constant for the reaction.
- Study the dependence of temperature on the reaction rate constant.
- Study the dependence of pressure on the reaction rate constant.
- Interpret the kinetic and activation parameters to understand the reaction mechanism.
- Study the effect of pH on the reaction rate constant when carried out in aqueous solution.

5. EXPERIMENTAL SECTION

5.1. CHEMICALS AND REAGENTS

The Fe(II) bis-thiosemicarbazone complexes $[\text{Fe}^{\text{II}}(\text{DpT})_2]$, $[\text{Fe}^{\text{II}}(\text{Dp44mT})_2]$, $[\text{Fe}^{\text{II}}(\text{ApT})_2]$ and $[\text{Fe}^{\text{II}}(\text{Ap4mT})_2]$ were provided at the beginning of this work by professor Paul V. Berndhardt (The University of Queensland, Australia) and were characterized in accordance with the literature methods.¹⁸⁻²¹

The reagents thiosemicarbazide, 4-methyl-3-thiosemicarbazide, 4,4-dimethyl-3-thiosemicarbazide, di(2-pyridil) ketone, 2-acetylpyridine and 2-benzoylpyridine were commercially available from Sigma-Aldrich. All solvents were AR Grade and used as received without further purification.

All buffer solutions were prepared using HEPES 0.2 M (approximate ionic strength 0.1 M) in a pH range from 6 to 8. They were degassed using a Schlenk line when needed oxygen-free.

5.1.1. Preparation of stock solutions

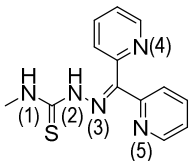
Stock solutions were prepared by dissolving 0.01 mmol of the $[\text{Fe}^{\text{II}}(\text{TSC})_2]$ complex in a Schlenk tube under N_2 atmosphere and carefully adding 2 cm^3 of degassed MeOH. The concentration of all stock solutions was thus 5 mM and they were stored at 0 °C for further use.

Air-saturated solvents and solutions were prepared by stirring at room temperature a 50 cm^3 aliquot that was kept stoppered for further use.

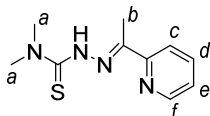
5.1.2. Thiosemicarbazone ligands: General procedure

The appropriate thiosemicarbazide (10 mmol) was dissolved in 10 cm^3 of distilled water, and the corresponding 2-pyridil ketone (HDpT series - Di(2-pyridyl) ketone, HBpT series - 2-Benzoylpyridine, HApT series - 2-Acetylpyridine; 10 mmol) was dissolved in 15 cm^3 of EtOH and added to the same round-bottom flask. Five drops of glacial acetic acid were added to the mixture, which was stirred and refluxed for 5 h. The flask was then cooled at room temperature

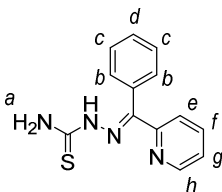
and stored overnight at 0 °C, the precipitate obtained was filtered and washed with EtOH and Diethyl ether.



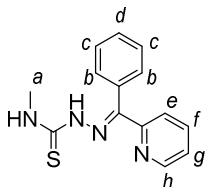
HDp4mT. Light yellow crystals (yield: 94%). $^1\text{H NMR}$ (DMSO- d_6 , 400 MHz): δ 8.82 (m, 1H, pyr), 8.56 (ddd, $J = 4.8, 1.7, 0.8$ Hz, 1H, pyr), 8.22(dt, $J = 7.9, 1.1$ Hz, 1H, pyr), 8.00-7.92 (m, 2H, pyr), 7.97 (m, 1H, pyr), 7.60-7.44 (overlap, 3H, pyr, $\text{HN}_{(1)}$), 3.06 (d, $J = 4.5$ Hz 3H, CH_3).



HAp44mT. Yellow needles (yield: 82%). $^1\text{H NMR}$ (DMSO- d_6 , 400 MHz): 8.76 (m, 1H, Hf), 8.58 (br d, 1H, $J_{gf} = 4.3$ Hz, Hc), 7.89-7.77 (overlap, 2H, Hd, He), 3.30 (s, 6H, Ha), 2.38 (d, 3H, $J = 10.6$ Hz, Hb).



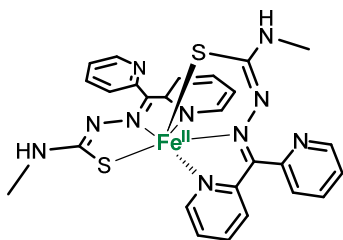
HBpT. Yellow powder (yield: 40%). $^1\text{H NMR}$ (DMSO- d_6 , 400 MHz): δ 8.86 (ddd, $J = 4.9, 2.3, 0.8$ Hz, 1H, Hh), 8.58 (m, 1H, He), 8.16 (m, 1H, Hf) 8.02 (td, $J = 7.9, 1.8$ Hz, 1H, Hg), 7.70-7.52 (overlap, 3H, Ha, Hb), 7.50-7.34 (overlapped, 3H, Hc, Hd).



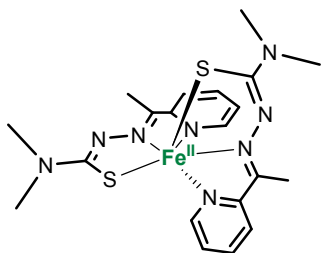
HBp4mT. Yellow powder (yield: 36%). $^1\text{H NMR}$ (DMSO- d_6 , 400 MHz): δ 8.78 (d, 1H, $J = 3.9$ Hz, Hh), 8.71 (m, 1H, He), 8.02 (m, 1H, Hf), 7.70-7.60 (overlapped, 3H, Hb, Hg), 7.52-7.42 (m, 3H, Hc, Hd), 3.04 (d, Ha).

5.1.3. Fe^{II} and Fe^{III} thiosemicarbazone complexes: General procedure

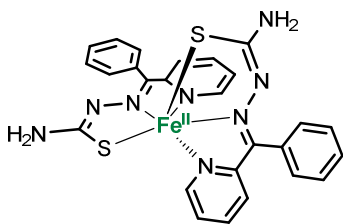
The thiosemicarbazone (3.2 mmol) was set in a Schlenk flask and purged with vacuum/ N_2 . 15 cm^3 of degassed EtOH was poured into the flask under counter-current of inert gas stream. 0.33 g (3.2 mmol) of Et_3N and 0.65 g (1.6 mmol) of $\text{Fe}(\text{ClO}_4)_2 \cdot x\text{H}_2\text{O}$ ($\text{Fe}(\text{ClO}_4)_3 \cdot 6\text{H}_2\text{O}$ for Fe^{III} complexes) was added using the same method. A condenser was connected to the Schlenk flask and the mixture was refluxed in nitrogen atmosphere for 1-2 h. After cooling at r.t, the precipitate obtained was filtered using a Schlenk-frit and washed with EtOH and diethyl ether.



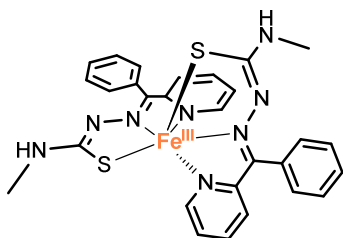
[Fe^{II}(Dp4mT)₂]. Dark green powder (yield: 90%). Electronic spectrum (MeOH): λ_{max} (nm) (ϵ , L mol⁻¹ cm⁻¹) 637 (8 710), 381 (27 370).



[Fe^{II}(Ap44mT)₂]. Green powder (yield: 93%). Electronic spectrum (MeOH): λ_{max} (nm) (ϵ , L mol⁻¹ cm⁻¹) 634 (560), 379 (27 280).



[Fe^{II}(BpT)₂]. Dark green powder (yield: 42%). Electronic spectrum (MeOH): λ_{max} (nm) (ϵ , L mol⁻¹ cm⁻¹) 641 (7 750), 365 (23 180).



[Fe^{III}(Bp4mT)₂]ClO₄. Brown powder (yield: 33%). Electronic spectrum (MeOH): λ_{max} (nm) (ϵ , L mol⁻¹ cm⁻¹) 475 (11 140), 378 (32 530).

5.2. PHYSICAL METHODS

NMR spectra were recorded with a Varian Mercury 400 MHz instrument at the Serveis Científics i Tecnològics de la Universitat de Barcelona in DMSO-d₆; the residual solvent signal was used as reference.

Electronic spectra were recorded using an Agilent G1103A UV-Vis spectrophotometer using degassed MeOH as solvent for the Fe(II) complexes. Table 1 collects the relevant UV-Vis characterization data of the complexes already available and prepared.

Cyclic voltammetry was also performed at the Serveis Científics i Tecnològics de la Universitat de Barcelona using a Biologic SP-150 potentiostat. A glassy carbon working electrode, a Ag/AgCl/3.0 M KCl Reference electrode and a Pt wire as the auxiliary electrode were used. The studied Fe^{II} and Fe^{III} complexes were dissolved in a mixture of MeCN:H₂O 70:30 (v/v); samples were prepared at an approximate concentration of 0.1 mM, with Bu₄NClO₄ (0.1 M) as the supporting electrolyte. All solutions were purged with nitrogen before registering the cyclic voltammograms. Data was recorded at a scan rate of 10 mV s⁻¹ in a range of potentials from -0.7 to 0.4 V. The redox potentials were given with respect to the normal hydrogen electrode (NHE) by adding 210 mV to the obtained values.

The pH was controlled using with a Crison pH & Ion-meter gip 22+.

Table 1. Characterization data of the Fe^{II} and Fe^{III} bis-thiosemicarbazone complexes already available and prepared.

Fe complex	λ_{\max_1} (nm)	λ_{\max_2} (nm)	E° [Fe ^{III} / II] /mV vs NHE
	(ϵ) (L mol ⁻¹ cm ⁻¹)	(ϵ) (L mol ⁻¹ cm ⁻¹)	
[Fe(ApT) ₂]	631 (2 380)	364 (14 040)	+12
[Fe(Ap4mT) ₂]	628 (270)	366 (11 330)	-10
[Fe(Ap44mT) ₂]	634 (560)	379 (27 280)	+57
[Fe(DpT) ₂]	644 (6 150)	338 (19 070)	+163
[Fe(Dp4mT) ₂]	637 (8 710)	381 (27 370)	+157
[Fe(Dp44mT) ₂]	646 (11 740)	383 (30 780)	Not determined
[Fe(BpT) ₂]	641 (7 750)	365 (23 180)	+115
[Fe(Bp4mT) ₂]ClO ₄	475 (11 140)	378 (32 530)	+110

5.3. KINETIC STUDIES

The kinetic experiments were carried out under pseudo-first order conditions: the concentration of the Fe(II) complex was chosen to be at least 10 times lower than the flooding concentration of O₂. By doing so, the concentration of O₂ remains constant during the experiments, which simplifies the rate law to a first-order form.

In all cases, the solutions used for experimentation were prepared by adding the calculated amounts of stock solutions of iron complex, degassed solvent, and air-saturated solvent. The mixture was then transferred to the measuring cell.

5.3.1. Variable-temperature kinetic experiments

The instrumentation used for variable-temperature kinetic experiments consisted in either an Agilent G1103A UV-Vis spectrophotometer connected to a Julabo MA-4 Class III heating circulator or a Varian Cary 50 UV-Vis spectrophotometer connected to a Julabo F32/MV thermostatic bath. Samples were set in quartz cuvettes and the monitoring of the experiments was taken in the 200-800 nm spectral region. The instruments provided a time resolved set of spectra that was analyzed with the adequate software.

5.3.2. Variable-pressure kinetic experiments

The kinetic experiments at variable pressure were performed in a range from 400 to 1800 atm using a J&M MMD/16 UV/500 spectrophotometer connected by fiber optics to a measurement block. A Polyscience circulating bath was used to control the fixed working temperature (20.6 °C) of this block.

The working pressures were attained by a system of water and oil connected to the steel block, where a pill-box cuvette with the sample was enclosed. The block also incorporated two 1 cm thick sapphire windows at each end where the fiber optics were connected using optical collimators. The resolved set of spectra provided by the instrument was analyzed with the corresponding software.

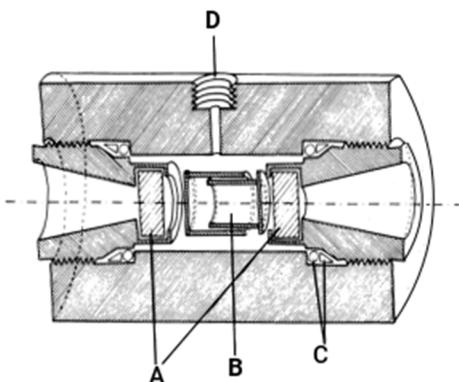


Figure 9. Diagram of the block used in the pressurizing System. A: Sapphire Windows, B: Pill-box cuvette, C: Pressurizing joints, D: Water inlet port for pressurization (Extracted from Vazquet et al., ref 22)

5.3.3. Software for data analysis

The data obtained from the time-resolved spectroscopic monitoring was treated with the Specfit32 and Reactlab™ Kinetics software. These programs allowed the time-resolved data to be fitted under pseudo-first order conditions to a single reaction step thus producing an observed rate constant for each experiment. The dependence of these values with the different concentration, temperature or pressure variables was conducted using OriginPro 8.

6. RESULTS

6.1. MODELLING THE TIME-RESOLVED SPECTRAL CHANGES: REACTION RATES

The oxidation of the studied Fe^{II} bis-thiosemicarbazone complexes by O₂ was studied in MeOH under the conditions mentioned in the experimental section. A decrease in the absorbance of the broad maximum around 640 nm, which corresponds to a Fe(II)-to-ligand charge transfer band was observed.²³ Other peaks in the UV region displayed a similar behavior, however, the mentioned CT band was used for kinetic studies due to a less important contribution of impurities in the visible region. The corresponding isosbestic points in the 450-500 nm region were used as a reference; this was particularly required for cases where solubility was an issue or a consequent decomposition process was evident.

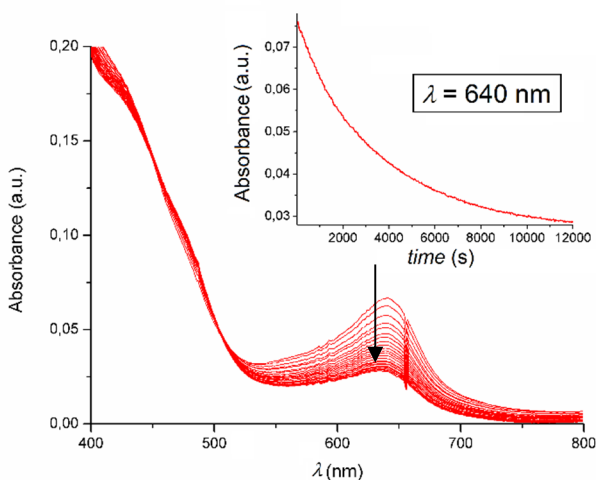


Figure 10. Changes in the electronic absorption spectrum of the species [Fe^{II}(Dp44mT)₂] in MeOH at a concentration of 0.01 mM, [O₂] = 2.15 mM, T = 15 °C, t = 12000 s.

The evolution of Fe^{II} complexes to their analogous Fe^{III} form was studied in a time frame typically ranging from 3600 to 16000 s. The DpT series required the longest periods of time for a complete reaction, followed by the ApT series. The complexes with the lowest reduction potentials, namely [Fe^{II}(Ap4mT)₂] and [Fe^{II}(Ap44mT)₂] required the shortest periods of measure.

The time-resolved spectral changes were modelled according to the experimental conditions of pseudo-first order conditions. Experiments were consistent with a single step (A→B) first-order reaction and data was fit to a single exponential change. In some cases, the simulation of a consecutive decomposition reaction was needed in order to obtain reliable and reproducible data.

The dependence of the observed pseudo-first-order reaction rate constant (k_{obs}) with the concentration of oxygen was studied in a range of O₂ concentrations from 0.43 to 2.15 mM at 15, 25 and 35 °C for the species [Fe^{II}(Dp44mT)₂]. This choice was based on the fact that this is the species with the highest reduction potential, as confirmed by cyclic voltammetry, thus allowing an easier time-resolved monitoring. At all temperatures, k_{obs} was linearly dependent with [O₂] and the slope of the graphs was used to obtain the second-order reaction rate constant (k) at the different working temperatures.

The linear concentration-dependence behavior observed was assumed for the rest of the complexes studied with the same working conditions. In this manner, the value of k_{obs} under air-saturated conditions was determined for the rest of the complexes and conditions; then, k_{obs} was divided by the O₂ concentration in air-saturated MeOH²³⁻²⁴ in order to obtain the second-order reaction rate constant (k). All complexes were also considered stable in MeOH, with no contribution to the rate constant at the zero of concentrations and the intercept was fixed accordingly.

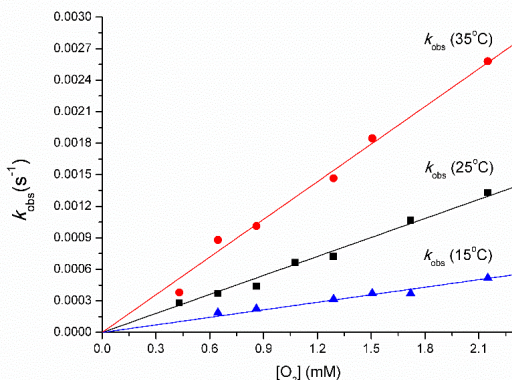


Figure 11. Variation of the observed pseudo-first-order reaction rate constant (k_{obs}) with the oxygen concentration in MeOH for the specie $[\text{Fe}^{\text{II}}(\text{Dp44mT})_2]$ at 15, 25 and 35 °C.

6.2. STUDY OF THE EFFECT OF TEMPERATURE

The Eyring equation is based on transition-state theory and illustrates the relationship between the reaction rate and the temperature. The linear form of the equation (Eqn 6) was used to determine the thermal activation parameters for the studied reactions, namely enthalpy (ΔH^\ddagger) and entropy of activation (ΔS^\ddagger). These parameters give important information on the nature of the reaction (electron transfer of the Fe^{II} complexes to the O_2 molecules in solution), as they help describe the characteristics of the activated complex.

$$\ln \left(\frac{k}{T} \right) = \ln \left(\frac{k_B}{h} \right) + \frac{\Delta S^\ddagger}{R} - \frac{\Delta H^\ddagger}{RT} \quad \text{Eqn. 6}$$

Where:

k_B : Boltzmann's constant.

h : Planck's constant.

R : Ideal gas constant.

The plot $\ln(k/T)$ versus $1/T$ (Fig. 12) produces an intercept that was used to obtain the value of ΔS^\ddagger and a slope from which ΔH^\ddagger can be derived (Eqn.6).

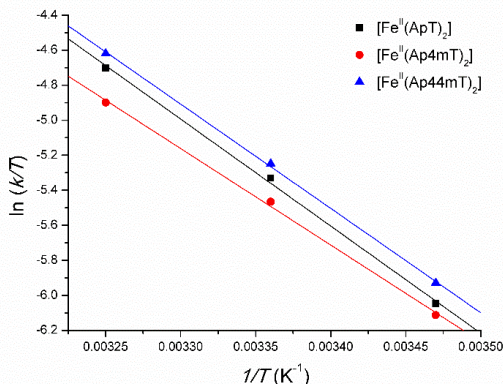


Figure 12. Eyring plot for the dependence of the rate constant on temperature for the Fe^{II} complexes of the ApT series in MeOH.

Table 2 collects the values of the activation parameters and the rate constants for all the species used in this study as estimated from the Eyring equation.

6.3. STUDY OF THE EFFECT OF PRESSURE

The relationship between the rate constant (k) and the hydrostatic pressure is described by the activation volume, Eqn 7. According to transition state theory, the volume of activation is interpreted as the change of partial volume on going from the reactants to the activated state. Negative values of ΔV^\ddagger correspond to an activated state with less volume than the reactants, and *vice versa*.²⁵ Pressure activation parameters were determined by measuring the rate constant at a fixed temperature over a wide range of pressures, as described in the experimental section.

$$\Delta V^\ddagger = -RT \left(\frac{\partial(\ln k)}{\partial P} \right)_T \quad \text{Eqn. 7}$$

The activation pressure parameters (ΔV^\ddagger) were thus obtained from a plot of $\ln k$ versus P (Fig. 13). For all reactions; in this case, a baseline correction in the isosbestic point was used for all the data analysis of the obtained time-resolved spectra. The value of k at $P = 1$ atm was also used as a reference, but never for calculations. Table 2 also collects the obtained values of ΔV^\ddagger for the Fe^{II} complexes used in this study.

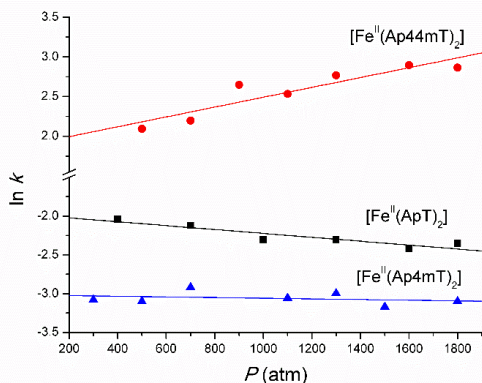
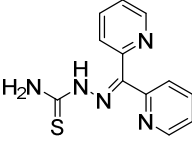
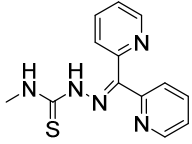
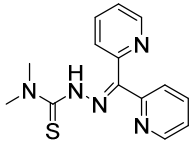
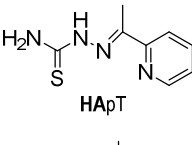
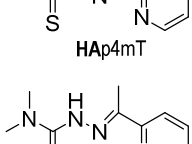



Figure 13. Plot of $\ln k$ versus P for the species $[\text{Fe}^{\text{II}}(\text{Ap44mT})_2]$ (red), $[\text{Fe}^{\text{II}}(\text{ApT})_2]$ (black) and $[\text{Fe}^{\text{II}}(\text{Ap4mT})_2]$ (blue). MeOH solution, $[\text{O}_2] = 2.15 \text{ mM}$, $T = 20.6 \text{ }^\circ\text{C}$

The TSC complexes with methyl substituents in the terminal nitrogen position showed, in all cases, positive values of ΔV^\ddagger , as opposed to the negative values of ΔS^\ddagger obtained for the same compounds. Conversely, the species with two H substituents in this position, showed a negative value of ΔV^\ddagger . The inverse relationship of the values found for ΔV^\ddagger and ΔS^\ddagger would suggest a formation of hydrogen bonds on going to the transition state. A clear dependence of the volume of activation and the number of protons in the N-terminal position was also found (Figure 13).

Table 2. Kinetic, Thermal and Pressure Activation Parameters for the Oxidation Processes of the [Fe^{II}(TSC)₂] complexes by O₂ in MeOH.

TSC Ligand	E' [Fe ^{III} / II] _{18,19} /mV vs NHE	²⁹⁸ (calc)k /M ⁻¹ s ⁻¹	ΔH ^P /kJ mol ⁻¹	ΔS ^P /J K ⁻¹ mol ⁻¹	ΔV ^P /cm ³ mol ⁻¹
 HDpT	+165	0.7	54±1	-70±3	3.0±0.2
 HDp4mT	+153	0.8	52±2	-75±5	-6±1
 HDp44mT	+166	0.7	57±5	-59±12	Not determined
 HApT	+20	1.3	49±3	-79±10	6±1
 HAp4mT	-3	1.1	48±2	-85±5	1±2
 HAp44mT	+49	1.6	49±1	-80±4	-14±3

6.4. STUDY OF THE EFFECT OF pH ON THE RATE CONSTANT IN AQUEOUS SOLUTIONS

Preliminary studies of the oxidation of the studied complexes by O_2 in H_2O (HEPES 0.2M, $I = 0.1$ M) were carried out for the $[Fe^{II}(DpT)_2]$ species at different pH values in the physiological range (6-8). In all cases, the solutions contained less than 1% of MeOH, which was originated from the stock solution of the complex. The concentration of O_2 was estimated by the corresponding concentration at air saturation (0.26 mM), in accordance with the literature.^{24,26} The values of the observed rate constants were studied following the procedures described in the experimental section, in a range of $[O_2]$ between 0.026-0.26 mM at 25 °C.

A decrease in the absorbance at the band with a maximum at 620 nm was observed, with the spectral changes corresponding to a set of two consecutive (A->B->C) reactions. Thus, the changes were fitted to a double exponential change (Fig. 14, left). The spectral changes displayed an important contribution of background noise in the 700-800 nm range due to poor solubility. Once the system was stabilized, a pseudo-first-order rate constant was obtained. As expected, this fact produced a set of values of k_{obs1} which included a large error effect, which makes their discussion only preliminary at this point.

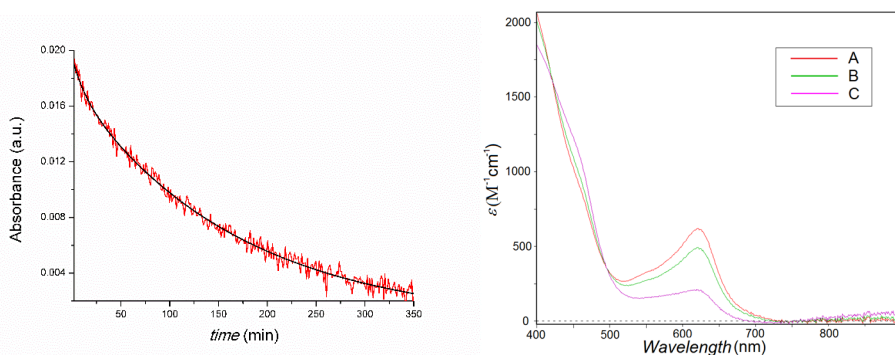


Figure 14. Left – Time-resolved absorption spectra at 620 nm of the species $[Fe^{II}(DpT)_2]$ in H_2O solution (pH = 7, HEPES 0.2M, $I = 0.1$ M, <1% MeOH), fitted with a double-exponential change. Right – SPECFIT-calculated concentration-time profiles derived from Fig.6, left.

A linear dependence between the concentration of oxygen in solution and the value of the observed pseudo-first-order rate constant was obtained as in methanol solution (Figure 15, left). From the slope of the k_{obs} versus $[O_2]$ plots the second-order rate constants was obtained, which roughly doubled with every decrease in unit of pH. The measurements also indicated the presence of an intercept at the zero of oxygen concentrations that also increased at low pH (Figure 15, right).

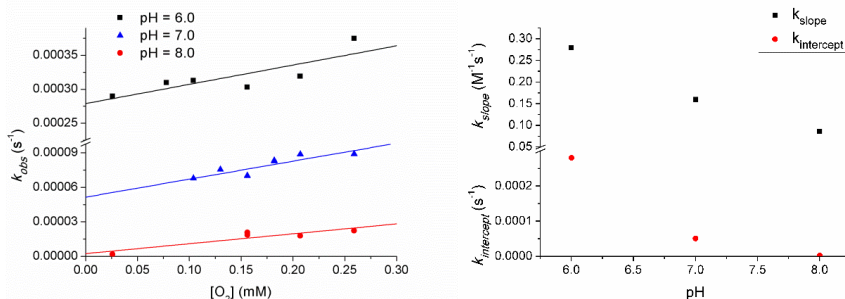
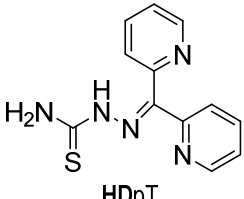


Figure 15. Left – Plot of the obtained pseudo-first-order rate constant ($k_{obs,2}$) versus $[O_2]$ in a range of pH from 6-8 for the species $[Fe^{II}(DpT)_2]$. $T=25^\circ C$. Right – Plot of k_{slope} and $k_{intercept}$ versus pH derived from (Fig.15, left).

Table 3. Kinetic parameters for the oxidation of the species $[Fe^{II}(DpT)_2]$ by O_2 in H_2O (HEPES 0.2 M, $I = 0.1$ M) $T = 25^\circ C$

TSC Ligand	pH	$^{298}(\text{calc})k_{slope}$ /M ⁻¹ s ⁻¹	$k_{intercept} \cdot 10^{-4}$ (s ⁻¹)
 HDpT	8.0	0.09±0.02	0.01±0.03
	7.0	0.14±0.03	0.55±0.05
	6.0	0.3±0.1	2.8±0.2

7. DISCUSSION

7.1. OBSERVED SPECTRAL CHANGES IN METHANOL SOLUTION

The electronic spectra of the series of studied Fe(II) complexes exhibited intense transitions in the 620-640 nm region, which are responsible of their characteristic green color. Previous structural characterization of the studied divalent and trivalent iron complexes by X-ray crystallography, have confirmed that both species have a slightly distorted octahedral geometry with rather short coordinate bond lengths, indicative of low spin configurations.^{18,19,27}

For the metal in its low oxidation state (electron-rich), obviously, this low energy transition can be assigned to a metal-to-ligand charge transfer (MLCT), *i.e.* a promotion of the electrons from an orbital of the metal into a ligand-based orbital, in this case, Fe^{II}→pyr.²⁰ Conversely, for the Fe(III) complexes an increase in the signal around 450 nm was observed, which indicates that the bands in this zone correspond to ligand-to-metal charge transfer (LMCT) transitions, responsible of the caramel color of the Fe^{III} species.

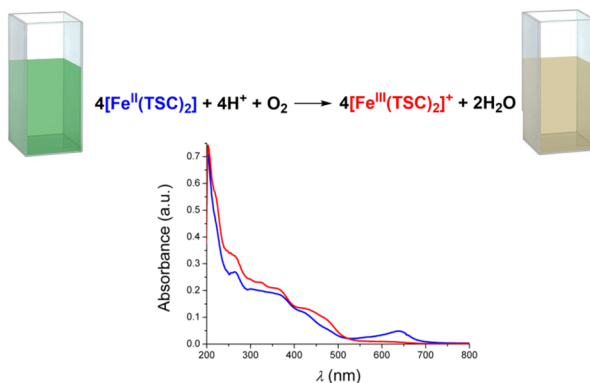


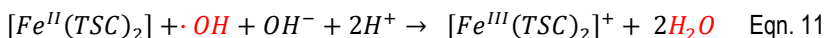
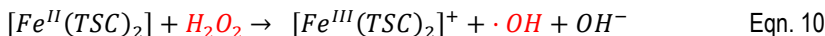
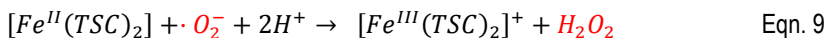
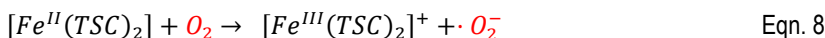
Figure 16. Observed spectral changes for the reaction of the species $[\text{Fe}^{\text{II}}(\text{DpT})_2]$ with O_2 in MeOH at initial reaction time (**blue**) and final (**red**, $t = 7200$ s). $[\text{O}_2] = 2.15$ mM, $[\text{complex}] = 0.1$ mM, $T = 15$ °C.

These transitions can be experimentally further identified as CT bands due to its observed negative solvatochromism. That is, the bands shift to lower wavelengths (higher energies) in water as compared to the less polar MeOH due to changes in the distribution of the electron density. Negative solvatochromism is a direct consequence of the Franck-Condon principle and is associated with important electronic dipole moment changes in the first solvation sphere of the complex with the MLCT transition.²⁸

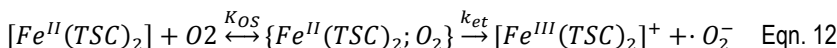
7.2. MECHANISTIC CLASSIFICATION

The mechanism of redox reactions for inorganic systems in solution can be classified as outer- or inner-sphere electron transfer. In our systems, despite not leading with an electron transfer between two metal centers, an inner-sphere mechanism can be disregarded since the Fe(II) complexes involved in this study are approximately t_{2g}^6 low spin (strong field). The coordination sphere having thus no labile coordination sites is not liable to be bound to the oxygen molecule in a reasonable time-scale.²⁹ The studied redox processes are consequently assumed to occur via an outer-sphere electron transfer mechanism

Despite being different systems, the aforementioned ability of Fe(II) bis-TSC complexes of reducing oxygen and releasing ROS species in cells⁶ can be used as a preliminary description of the observed reactions by using the following chemical equations:



Given the fact that a single step was observed for the process, Eqn. 8 or 10 could be used as the determining step following this hypothesis, despite the existence of obvious multiple electron transfer processes that do not appear to be rate-determining. In this way, the contribution of k_1 or k_3 to the apparent rate constant obtained would be the most important of all the reactions. If Eqn. 8 was the rate-determining step the following OS would take place:



With the equation of the observed reaction rate constant being of the form:

$$k_{obs} = \frac{K_{OS} k_{et} [O_2]}{1 + K_{OS} [O_2]} \quad \text{Eqn. 13}$$

This equation indicates that a curvature in the plot of k_{obs} vs $[O_2]$ would be expected at high oxidant concentrations. However, this behavior is not observed in none of the studied systems, which indicates that either the value of the outer-sphere complex formation constant is rather low, or the value of $[O_2]$ is too low for its detection. Consequently, the equation simplifies the denominator ($1 + K_{OS} [O_2]$) to unity.³⁰ Probably the fact that the oxygen concentrations used had to be kept in the low side due to its solubility represents the actual reason for the behavior observed.

7.3. RELATION OF THE KINETIC AND ACTIVATION PARAMETERS WITH THE STANDARD REDUCTION POTENTIAL IN METHANOL SOLUTION

The values of the standard reduction potentials were obtained by cyclic voltammetry as described in the experimental section and agree with those reported in the literature.^{18,19} The range of reduction potentials of the studied complexes was fairly broad ($-3 < E^{\circ}$ (mV versus NHE) < 166), with all the species being redox-active. In all cases, the redox potentials could easily be related to the energy of the above mentioned MLCT transitions.²⁰

The ApT Fe(II) series of complexes is exhibit the lowest reduction potentials, and thus a more thermodynamically-favored oxidation of its Fe^{II} complexes, followed by DpT series. These changes in the E° values have already been associated to the inductive effects of the carbonyl compound precursors (di-2-pyridil ketone, and 2-acetylpyridine). That is, the highest reduction potentials of the DpT series are due to the electron withdrawing effect of the pyridyl group that is not coordinated with the metal.²⁸ Within the same series, the change in reduction potential on increasing the number of methyl substituents in the amine groups is not very evident, and it could be related to a combination of electronic and steric effects.³¹

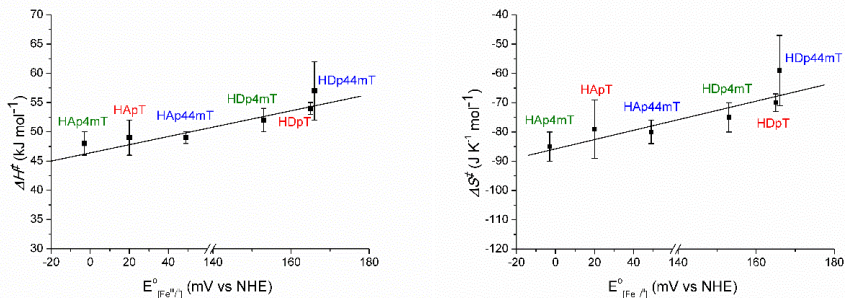


Figure 17. Plot of the thermal activation parameters, ΔH^\ddagger (left) and ΔS^\ddagger (right) versus $E^0_{[Fe^{II}/Fe^{III}]}$ (mV versus NHE). MeOH solution.

The relationship between the obtained kinetic and activation parameters and the reduction potential of the species utilized has also been studied (Fig. 17). The large values determined for the activation enthalpy in the 60–45 kJ mol $^{-1}$ range (Table 2), indicates that the electron transfer process is rather enthalpy demanding³² and the negative values of ΔS^\ddagger indicate that there is a substantial degree of ordering on going to the transition state from the reactants.³³ For the latter, one should note that, as indicated before (Eqn. 13), the second order rate constant corresponds to the product $K_{os} \cdot k_{et}$, thus the formation of the outer-sphere complexes being included in the determined activation parameters, which is specially significant for the entropy terms.³⁰

The values of the second order reaction rate constants (Table 2) show a clear positive correlation with the reduction potential, which suggests that this is an important factor for the increase in velocity of the reaction. That is, electronic and steric effects play a determinant role in the process, as expected for outer-sphere redox processes.^{32–33} Previous kinetic studies of the oxidation of the analogous Fe III complexes by HbO $_2$, found no definite correlation between the standard reduction potentials and the reaction rate constants. Even though the range of potentials was as wide as in this study, the fact that the reactions were rather site-specific has been related to the fact that H-bonding interactions represented a crucial factor for these systems.²⁹

In view of the data previously published about the reaction of the Fe III species with HbO $_2$, the values of ΔV^\ddagger were scanned carefully for significant differences with structural changes on the terminal amine group. Effectively, for the complexes with no substituents in the N-terminal position the values found are clearly positive, whereas for the species having a fully methylated

amine group the value found is negative; for the systems with a single methyl group in the N-terminal position, intermediate values were obtained (Fig.18).

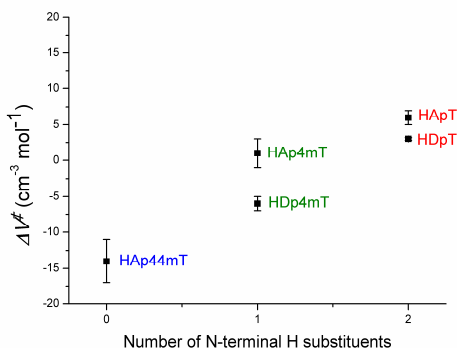


Figure 18. Plot of the baric activation parameters (ΔV^\ddagger) versus the N-terminal H substituents for the studied ferrous complexes.

For all the complexes with amine unsubstituted thiosemicarbazone ligands, the values clearly indicate a neat expansion of the systems on going to the transition state, which is opposite to the ordering indicated by the values of the measured activation entropies. Contrarily, for the fully substituted Ap44mT ligand the value determined is rather negative, in line with the value of ΔS^\ddagger , which would be expected from a simplistic approach.³⁴ This difference in behavior suggests that the formation of hydrogen bonds on going from the reactants to the transition state plays a determinant role in the mechanism, as suggested before. We can speculate about the fact that the protons in the amine groups of the ligands and the lone pairs of the oxygen molecule do have an expansion/ordering effect in the process as found for a plethora of other systems studied.^{33,35} Figure 19 represents a simplified view of the proposed possible interactions which also explains the intermediate behavior of the single methylated ligand complexes.

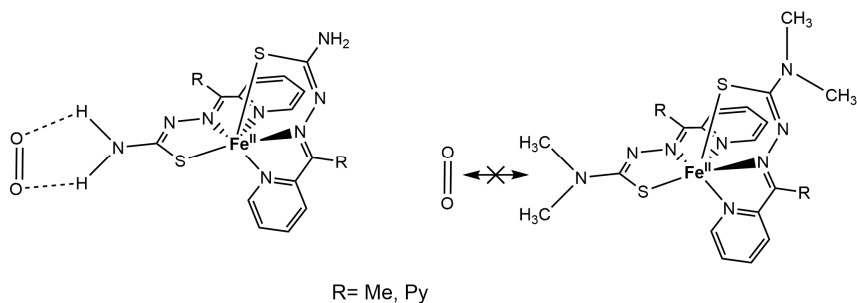


Figure 19. Illustration of H-bonding between dioxygen and the protons in the amine groups of the ligands on going to the transition state. Adapted from Basha et. al, ref 29

7.4. INTERPRETATION OF THE EFFECT OF pH ON THE RATE CONSTANT IN AQUEOUS SOLUTIONS

As observed by the obtained values of the second-order rate constant in aqueous solution at pHs close to physiological levels (Table 3), the reactions were substantially slower compared to methanol solution, in line with the 10-fold decrease in oxygen concentrations. Furthermore, the dependence of the determined second-order rate constant with pH is evident (Fig 15, left), roughly doubling with every pH unit, indicating the involvement of protons in the reaction.

Previously reported data suggested the formation of peroxides during the reaction monitored.²⁹ In fact, bubbles were observed once the reactions were finished (Fig. 20), which was more apparent for samples at higher concentrations of O₂. However, this observation should be considered cautiously, as the amount of data so far is insufficient to give any complete credibility to these claims. Future studies should allow a better insight of the reaction mechanism.

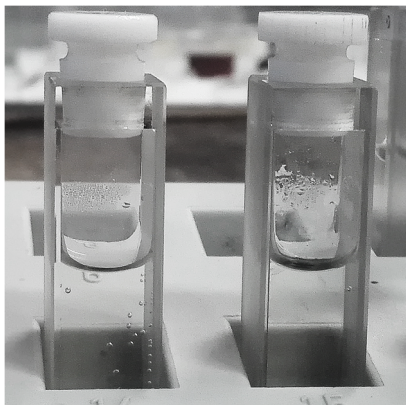


Figure 20. Cuvettes with the samples after monitoring the reaction for the species $[\text{Fe}^{\text{II}}(\text{DpT})_2]$ at 25 °C, pH = 7.0. Left – $[\text{O}_2] = 0.26 \text{ mM}$ Right – 0.05 mM .

8. CONCLUSIONS

The kinetic studies of the oxidation of Fe(II) bis-thiosemicarbazone complexes by O₂ in MeOH solution in a temperature-range from 15 to 35 °C and pressures ranging from 1 to 2000 atm have been conducted. Preliminary studies in aqueous solutions at physiological levels of pH have also been conducted.

The time-resolved set of electronic spectra in MeOH determined indicate that only one step is rate determining for these reactions. In aqueous solutions, secondary reactions were also observed, but were not considered to be part of the studied process as a result of to the large inherent error due to the concentrations used.

A determinant influence of structural factors of the ligands related to hydrogen bonding and steric/electronic influences was observed in methanol solutions. Although hydrogen bonding seemed to be an important aspect in the formation of the outer-sphere complexes and reactant orientations, steric and electronic effects are the most crucial factors in the velocity of the reaction. This is clearly quantified by the direct relationship of the second-order rate constant with the standard reduction potentials of the complexes studied.

The aqueous solution kinetic experiments determined at varying pH confirm the importance of protons in the reaction medium. The possible formation of hydrogen peroxide, however, has only been considered as a preliminary observation due to insufficient reliable and reproducible data. Future experiments will have to shed light on the characteristics of these chemical reactions and their mechanism in aqueous solution.

9. REFERENCES AND NOTES

1. Opletalová, V.; Kalinowski, D. Identification and Characterization of Thiosemicarbazones with Antifungal and Antitumor Effects: Cellular Iron Chelation Mediating Cytotoxic Activity. *Chem. Res. Toxicol.* **2008**, *21*, 1878–1889.
2. Kalinowski, D. S.; Kovacevic, Z.; Siafakas, A. R.; Jansson, P. J.; Stefani, C.; Lovejoy, D. B.; Sharpe, P. C.; Bernhardt, P. V.; Richardson, D. R. Thiosemicarbazones from the Old to New: Iron Chelators That Are More than Just Ribonucleotide Reductase Inhibitors. *J. Med. Chem.* **2009**, *52* (17), 5271–5294.
3. Cooper, C. E.; Lynagh, G. R.; Hoyes, K. P.; Hider, R. C.; Cammack, R.; Porter, J. B. The Relationship of Intracellular Iron Chelation to the Inhibition and Regeneration of Human Ribonucleotide Reductase. *J. Biol. Chem.* **1996**, *271* (34), 20291–20299.
4. Yu, Y.; Gutierrez, E.; Kovacevic, Z.; Saletta, F.; Obeidy, P.; Suryo Rahmanto, Y.; Richardson, D. R. Iron Chelators for the Treatment of Cancer. *Curr. Med. Chem.* **2012**, *19*, 2689–2702.
5. Crisponi, G.; Remelli, M. Iron Chelating Agents for the Treatment of Iron Overload. *Coord. Chem. Rev.* **2008**, *252* (10–11), 1225–1240.
6. Jansson, P. J.; Kalinowski, D. S.; Lane, D. J. R.; Kovacevic, Z.; Seebacher, N. A.; Fouani, L.; Sahni, S.; Merlot, A. M.; Richardson, D. R. The Renaissance of Polypharmacology in the Development of Anti-Cancer Therapeutics: Inhibition of The “triad of Death” in Cancer by Di-2-Pyridylketone Thiosemicarbazones. *Pharmacol. Res.* **2015**, *100*, 255–260
7. Kalinowski, D. S.; Richardson, D. R. Future of toxicology iron chelators and differing modes of action and toxicity: the changing face of iron chelation therapy. *Chem. Res. Toxicol.* **2007**, *20*, 715–720
8. Kalinowski, D. S.; Sharpe, P. C.; Islam, M.; Liao, Y.; Lovejoy, D. B.; Kumar, N.; Bernhardt, P. V.; Richardson, D. R. Design, Synthesis, and Characterization of Novel Iron Chelators: Structure – Activity Relationships of the 2-Benzoylpyridine Thiosemicarbazone Series and Their 3-Nitrobenzoyl Analogues as Potent Antitumor Agents. *Society* **2007**, 3716–3729.
9. (Lancashire R.J, Awan A., Truong H. Crystal Field Theory. *Chemistry Libre Texts*. [Online] http://chem.libretexts.org/Core/Inorganic_Chemistry/Crystal_Field_Theory/Crystal_Field_Theory (accessed December 20, 2016).
10. Atkins, P; Overton, T; Rourke J; Weller M.; Armstrong F. Complejos de los metales d: estructura electrónica y espectros. Química inorgánica, Cuarta edición; Mc-Graw-Hill Interamericana; México, D.F.; **2008**; pp 479-482.
11. Gold, V. COMMISSION ON PHYSICAL ORGANIC CHEMISTRY * GLOSSARY OF TERMS USED IN Compiled and Edited by. *Pure Appl. Chem.* **1979**, *51* (5), 1731.
12. Pillings, M.J; Seakins P.W. Reaction Kinetics; Oxford Univeristy Press, Inc; New York; 1996; pp 170-173.
13. Jordan, B. R. Reaction Mechanisms of Inorganic and Organometallic Systems; Oxford University Press, Inc; New York, **1991**; pp. 167-197.
14. Holliday, B. J.; Swager, T. M. Conducting Metallopolymers: The Roles of Molecular Architecture and Redox Matching. *Chem. Commun. (Camb)*. **2005**, No. 1, 23–36.
15. Siders, P.; Marcus, R. A. Quantum Effects in Electron-Transfer Reactions. *J. Am. Chem. Soc.* **1981**, *103* (4), 741–747.

16. Marcus, R. A.; Sridhar, P. Theory of Electron Transfer Reactions and Comparison with Experiments. In *Photoprocesses in Transition Metal Complexes, Biosystems and Other Molecules*. Experiment and Theory; Kochanski, E., Ed.; Springer Netherlands: Dordrecht, **1992**; pp 49–88.
17. Lippin, G; *Redox Mechanisms in Inorganic Chemistry*; Ellis Horwood; Great Britain; **1994**; pp 77-82.
18. Kalinowski, D. S.; Sharpe, P. C.; Islam, M.; Liao, Y.; Lovejoy, D. B.; Kumar, N.; Bernhardt, P. V.; Richardson, D. R. Design, Synthesis, and Characterization of Novel Iron Chelators: Structure – Activity Relationships of the 2-Benzoylpyridine Thiosemicarbazone Series and Their 3-Nitrobenzoyl Analogues as Potent Antitumor Agents. *J. Med. Chem* **2007**, 3716–3729.
19. Richardson, D. R.; Kalinowski, D. S.; Richardson, V.; Sharpe, P. C.; Lovejoy, D. B.; Islam, M.; Bernhardt, P. V. 2-Acetylpyridine Thiosemicarbazones Are Potent Iron Chelators and Antiproliferative Agents: Redox Activity, Iron Complexation and Characterization of Their Antitumor Activity. *J. Med. Chem.* **2009**, 52 (5), 1459–1470.
20. Richardson, D. R.; Sharpe, P. C.; Lovejoy, D. B.; Senaratne, D.; Kalinowski, D. S.; Islam, M.; Bernhardt, P. V. Dipyriddy Thiosemicarbazone Chelators with Potent and Selective Antitumor Activity Form Iron Complexes with Redox Activity. *J. Med. Chem.* **2006**, 49 (22), 6510–6521.
21. Bernhardt, P. V.; Martínez, M.; Rodríguez, C.; Vázquez, M. Biologically Active Thiosemicarbazone Fe Chelators and their Reactions with Ferrioxamine B and Ferric EDTA; a Kinetic Study. *Dalton Trans.* **2012**, 41, 2122-2130.
22. Vázquez, M. Estudio cinético de la interacción de complejos de metales de transición con moléculas biológicamente relevantes. Ph.D Thesis, University of Barcelona, 2016.
23. Quaranta, M.; Murkovic, M.; Klimant, I. A New Method to Measure Oxygen Solubility in Organic Solvents through Optical Oxygen Sensing. *Analyst* **2013**, 138 (21), 6243–6245.
24. Sato, T.; Hamada, Y.; Sumikawa, M.; Araki, S.; Yamamoto, H. Solubility of Oxygen in Organic Solvents and Calculation of the Hansen Solubility Parameters of Oxygen. *Ind. Eng. Chem. Res.* **2014**, 53 (49), 19331–19337.
25. Avery, H.E. *Basic Reaction kinetics and mechanisms*; The Macmillan press Ltd; London and Basingstoke; 1974; pp. 109-112.
26. Wilhelm, E.; Battino, R.; Wilcock, R. J. Low-Pressure Solubility of Gases in Liquid Water. *Chem. Rev.* **1977**, 77, 219–262.
27. Bernhardt, P. V.; Sharpe, P. C.; Islam, M.; Lovejoy, D. B.; Kalinowski, D. S.; Richardson, D. R. Iron Chelators of the Dipyriddyketone Thiosemicarbazone Class: Precomplexation and Transmetalation Effects on Anticancer Activity. *J. Med. Chem.* **2009**, 52 (2), 407–415. 15
28. Manuta, D. M.; Lees, A. J. Solvatochromism of the Metal to Ligand Charge-Transfer Transitions of Zerovalent Tungsten Carbonyl Complexes. *Inorg. Chem.* **1986**, 25 (May), 3212–3218.
29. Basha, M. T.; Bordini, J.; Richardson, D. R.; Martínez, M.; Bernhardt, P. V. Kinetic-Mechanistic Studies on Methemoglobin Generation by Biologically Active Thiosemicarbazone iron(III) Complexes. *J. Inorg. Biochem.* **2016**, 162, 326–333.
30. Martínez, M.; Vázquez, M. Kinetic-Mechanistic Studies of Nucleoside and Nucleotide Substitution Reactions of Co(III) Complexes of Fully Alkylated Cyclen. *Inorg. Chem.* **2015**, 54 (10), 4972–4980.
31. Schmidt, M.; Miskelly, G.; Lewis, N. Effects of Redox Potential, Steric Configuration, Solvent, and Alkali Metal Cations on the Binding of Carbon Dioxide to cobalt(I) and nickel(I) Macrocycles. *J. Am. Chem. Soc.* **1990**, 112 (9), 3420–3426.
32. Martínez, M.; Pitarque, M.-A.; van Eldik, R. Outer-Sphere Redox Reactions of (N)5-Macrocyclic cobalt(III) Complexes. A Temperature and Pressure Dependence Kinetic Study on the Influence of Size and Geometry of Different Macrocycles. *Inorganica Chim. Acta* **1997**, 256 (1), 51–59.
33. Granell, J.; Martínez, M. Kinetic-Mechanistic Studies of Cyclometalating C–H Bond Activation Reactions on Pd(II) and Rh(II) Centres: The Importance of Non-Innocent Acidic Solvents in the Process. *Dalt. Trans.* **2012**, 41 (37), 11243.
34. Van Eldik, R. Mechanistic Studies in Coordination Chemistry. *Coord. Chem. Rev.* **1999**, 182, 373–410.

35. Bernhardt, P. V.; Bozoglian, F.; Macpherson, B. P.; Martinez, M.; Merbach, E.; Gonzalez, G.; Sienna, B.; Polytechnique, A. Oxidation of Mixed-Valence Co III / Fe II Complexes Reversed at High pH: A Kinetic-Mechanistic Study of Water Oxidation. *Inorg. Chem.* **2004**, 43 (22), 7187–7195.

10. ACRONYMS

TSC: Thiosemicarbazone

ROS: Reactive oxygen species

RR: Ribonucleotide reductase

CT: Charge-transfer

MLCT: Metal-to-ligand charge transfer

NHE: Normal hydrogen electrode

AR: Standard Mallinckrodt grade of analytical reagents

OS: Outer-sphere

HApT: 2-acetylpyridine thiosemicarbazone

HAp4mT: 2-acetylpyridine 4-methylthiosemicarbazone

Hap44mT: 2-acetylpyridine 4,4-dimethylthiosemicarbazone

HDpT: di-2-pyridyl thiosemicarbazone

HDp4mT: di-2-pyridyl 4-methylthiosemicarbazone

HDp44mT: di-2-pyridyl 4,4-dimethylthiosemicarbazone

HBpT: 2-benzoylpyridine thiosemicarbazone

HBp4mT: 2-benzoylpyridine 4-methylthiosemicarbazone

APPENDICES

APPENDIX 1: DATA USED FOR KINETIC STUDIES ON THE TEMPERATURE DEPENDENCE IN MeOH SOLUTIONS

[Fe^{II}(Dp44mT)₂] – Data for the study of the relationship between k_{obs} and [O₂] in MeOH

[O ₂] (mM)	k_{obs} (s ⁻¹)		
	25 °C	35 °C	15 °C
0.43	2.81E-04	3.80E-04	--
0.65	3.70E-04	8.81E-04	1.87E-04
0.86	4.39E-04	1.01E-03	2.24E-04
1.08	6.65E-04	--	--
1.29	7.23E-04	1.47E-03	3.16E-04
1.51	--	1.85E-03	3.71E-04
1.72	1.07E-03	--	3.70E-04
2.15	1.33E-03	2.58E-03	5.18E-04

[Fe^{II}(Dp4mT)₂] – Kinetic data (average values) used for the Eyring plot. MeOH solution

T (°C)	k_{obs} (s⁻¹)	k (M⁻¹ s⁻¹)	1/T (°K⁻¹)	ln (k/T)
15	8.11E-04	0.38	0.00347	-6.63
25	1.66E-03	0.77	0.00336	-5.96
35	3.51E-03	1.63	0.00325	-5.23

[Fe^{II}(DpT)₂] – Kinetic data (average values) used for the Eyring plot. MeOH solution.

T (°C)	k_{obs} (s⁻¹)	k (M⁻¹ s⁻¹)	1/T (°K⁻¹)	ln (k/T)
15	7.32E-04	0.34	0.00347	-6.74
25	1.63E-03	0.76	0.00336	-5.98
35	3.26E-03	1.52	0.00325	-5.31

[Fe^{II}(Ap44mT)₂] – Kinetic data (average values) used for the Eyring plot. MeOH solution

T (°C)	k_{obs} (s⁻¹)	k (M⁻¹ s⁻¹)	1/T (°K⁻¹)	ln (k/T)
15	1.71E-03	0.80	0.00347	-5.89
25	3.33E-03	1.55	0.00336	-5.26
35	6.55E-03	3.05	0.00325	-4.61

[Fe^{II}(Ap4mT)₂] – Kinetic data (average values) used for the Eyring plot. MeOH solution

T (°C)	k_{obs} (s⁻¹)	k (M⁻¹ s⁻¹)	1/T (°K⁻¹)	ln (k/T)
15	1.34E-03	0.62	0.00347	-6.14
25	2.78E-03	1.29	0.00336	-5.44
35	5.15E-03	2.40	0.00325	-4.86

[Fe^{II}(Ap4T)₂] – Kinetic data (average values) used for the Eyring plot. MeOH

T (°C)	k_{obs} (s⁻¹)	k (M⁻¹ s⁻¹)	1/T (°K⁻¹)	ln (k/T)
15	1.47E-03	0.68	0.00347	-6.04
25	2.48E-03	1.15	0.00336	-5.30
35	5.15E-03	2.40	0.00325	-4.68

APPENDIX 2: DATA USED FOR PRELIMINARY STUDIES ON THE RELATIONSHIP BETWEEN THE RATE CONSTANT AND pH IN AQUEOUS SOLUTION

[Fe^{II}(DpT)₂] : HEPES 0.2 M, I = 0.1 M , pH = 6.0, T=25 °C, <1% MeOH

[O ₂] (mM)	K _{obs,1} (s ⁻¹)	K _{obs,2} (s ⁻¹)
0.078	--	3.095E-04
0.010	3.11E-04	3.13E-04
0.16	4.30E-04	3.03E-04
0.18	5.24E-04	--
0.21	7.54E-04	3.19E-04
0.26	7.79E-04	3.75E-04

[Fe^{II}(DpT)₂] : HEPES 0.2 M, I = 0.1 M, pH = 7.0, T=25 °C, <1% MeOH

[O ₂] (mM)	K _{obs,1} (s ⁻¹)	K _{obs,2} (s ⁻¹)
0.026	3.56E-04	--
0.052	3.45E-04	--
0.10	3.54E-04	6.80E-05
0.13	4.02E-04	7.54E-05
0.18	--	8.32E-05
0.21	6.78E-04	8.87E-05
0.26	7.41E-04	8.90E-05

[Fe^{II}(DpT)₂] : HEPES 0.2 M, I = 0.1 M, pH = 8.0, T=25 °C, <1% MeOH

[O ₂] (mM)	K _{obs,1} (s ⁻¹)	K _{obs,2} (s ⁻¹)
0.026	--	1.8E-06
0.052	1.51E-03	--
0.10	2.00E-03	--
0.16	1.98E-03	1.855E-05
0.21	2.26E-03	1.7833E-05
0.26	2.57E-03	2.23E-05

